INTERNATIONAL JOURNAL FOR NUMERICAL METHODS IN ENGINEERING
Int. J. Numer. Meth. Engng 2005; **63**:276–289
Published online 21 February 2005 in Wiley InterScience (www.interscience.wiley.com). DOI: 10.1002/nme.1286

A finite element method for the computational modelling of cohesive cracks

J. Mergheim, E. Kuhl and P. Steinmann*, †

Chair of Applied Mechanics, Department of Mechanical Engineering, University of Kaiserslautern, P.O. Box 3049, 67653 Kaiserslautern, Germany

SUMMARY

The present contribution is concerned with the computational modelling of cohesive cracks in quasi-brittle materials, whereby the discontinuity is not limited to interelement boundaries, but is allowed to propagate freely through the elements. In the elements, which are intersected by the discontinuity, additional displacement degrees of freedom are introduced at the existing nodes. Therefore, two independent copies of the standard basis functions are used. One set is put to zero on one side of the discontinuity, while it takes its usual values on the opposite side, and *vice versa* for the other set. To model inelastic material behaviour, a discrete damage-type constitutive model is applied, formulated in terms of displacements and tractions at the surface.

Some details on the numerical implementation are given, concerning the failure criterion, the determination of the direction of the discontinuity and the integration scheme. Finally, numerical examples show the performance of the method. Copyright © 2005 John Wiley & Sons, Ltd.

KEY WORDS: discontinuous elements; cohesive cracks; propagating discontinuities

1. INTRODUCTION

In the present paper, a method for the modelling of cohesive cracks is described. The discontinuity is supposed to propagate independently of the mesh structure. Therefore, elements with an internal discontinuity are formulated. The construction of these elements follows the approach, recently proposed by Hansbo and Hansbo in References [1, 2]. To model inelastic material behaviour, a discrete damage-type model is applied, formulated in terms of displacements and tractions at the discontinuity surface. The discontinuities are introduced when a failure criterion is met, such that the discrete constitutive model characterizes the inelastic behaviour only and the continuum represents the elastic response.

*Correspondence to: P. Steinmann, Chair of Applied Mechanics, Department of Mechanical Engineering, University of Kaiserslautern, P.O. Box 3049, 67653 Kaiserslautern, Germany.
†E-mail: ps@rhrk.uni-kl.de

Contract/grant sponsor: German Science Foundation; contract/grant number: DFG Graduiertenkolleg 814

Received 7 May 2004
Revised 2 September 2004
Accepted 17 November 2004

The modelling of strong discontinuities that can run arbitrarily through finite elements was considered by several authors over the past years. Mainly two formulations can be distinguished: elements with embedded discontinuities and extended finite element methods, based on the partition of unity method [3].

In the approach with embedded discontinuities, strain or displacement discontinuities are inserted by means of additional degrees of freedom on the element level. This permits the discontinuity to have arbitrary orientation. The class of methods seems to go back to References [4, 5]. For the geometrically linear case, finite element methods with embedded discontinuities have been presented, for example in the References [6, 7], and an extension to finite strains can be found in References [8, 9].

The extended finite element method, which is conceptually most similar to the present one, traces back to Belytschko *et al.*; see References [10, 11]. The essential idea of the method is to add enrichment functions to the approximation, which contain a discontinuous displacement field. The method was shown to be capable of handling three-dimensional cracks [12] and intersecting and branching cracks [13]. Wells and Sluys [14] and Zi and Belytschko [15] applied the partition of unity method to the modelling of cohesive cracks.

The special characteristic of the present approach lies in the formulation of the elements with internal discontinuities, which is based on References [1, 2]. In contrast to the present method, in References [1, 2], the discontinuous elements were applied in an extended Nitsche's method [16]. This allows for the simulation of weak as well as strong discontinuities within the elements, but the formulation was restricted to a linear traction-separation law.

The displacement field of an intersected element is a discontinuous function, which exhibits a jump along the discontinuity, but is continuous on both sides of this discontinuity. Therefore, the displacement field can also be considered as two independent continuous functions, with the displacement jump being the difference of the two function values at both sides of the discontinuity. Additional displacement degrees of freedom are introduced at the existing nodes and two independent copies of the standard basis functions are used to permit the approximation of the two continuous functions. One set of basis functions is put to zero on one side of the discontinuity, while it takes its usual values on the other side and *vice versa*. This allows for the formulation of elements with an internal discontinuity, using only displacement degrees of freedom and the standard basis functions. In the opinion of the authors, the present approach is conceptually simpler than the X-FEM, although it eventually leads to quite a similar formulation and comparable results. Since it does not work with the displacement jump as an explicit variable, the approach resembles more traditional finite element methods.

In the next section, the kinematic relations for a domain crossed by a discontinuity are described. Thereafter, the governing equations are recapitulated and the weak formulation is given, which is followed by the characterization of the applied constitutive laws. Then the spatial discretization and the construction of the elements with an internal discontinuity are specified. Afterwards, some details concerning the implementation are given and the performance of the method is pointed out by means of numerical examples. The paper closes with a conclusion.

2. KINEMATICS

Let $\Omega \subset \mathbb{R}^{n_{\mathrm{dim}}}$ denote the configuration occupied by an initially linear elastic body with placements in $\mathbb{R}^{n_{\mathrm{dim}}}$ denoted by $\mathbf{x}$. The boundary $\partial\Omega$ of Ω with the outward normal $\mathbf{n}_{\mathrm{e}}$ is

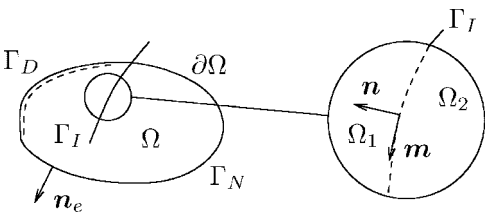

Figure 1. Domain Ω crossed by a discontinuity Γ_{I}.

subdivided into disjoint parts $\partial\Omega = \Gamma_{\mathrm{N}} \cup \Gamma_{\mathrm{D}}$ with $\Gamma_{\mathrm{N}} \cap \Gamma_{\mathrm{D}} = \emptyset$, where either Neumann or Dirichlet boundary conditions are prescribed. Furthermore, Ω exhibits a smooth internal boundary Γ_{I}, which divides Ω into the parts Ω_1 and Ω_2. The unit normal vector $\mathbf{n}$, associated with Γ_{I}, points from Ω_2 to Ω_1, and the tangential vector to Γ_{I} is denoted with $\mathbf{m}$, as is pictured in Figure 1.

The displacement field $\mathbf{u}$ is discontinuous along Γ_{I} but continuous on Ω_1 and Ω_2. Therefore, $\mathbf{u}$ can be represented by two continuous functions $\mathbf{u}_1$ and $\mathbf{u}_2$

$$\mathbf{u}(\mathbf{x}) = \begin{cases} \mathbf{u}_1(\mathbf{x}) & \text{in } \Omega_1 \\ \mathbf{u}_2(\mathbf{x}) & \text{in } \Omega_2 \end{cases} \tag{1}$$

whereby $\mathbf{x}$ denotes the position of the material point. The jump in the displacement field $[\![\mathbf{u}]\!]$ can then be derived by

$$[\![\mathbf{u}]\!] = \mathbf{u}_1 - \mathbf{u}_2 \quad \text{on } \Gamma_{\mathrm{I}} \tag{2}$$

The strain field in the bulk is found by taking the derivative of the displacement field. For the considered geometrically linear case the strain tensor $\boldsymbol{\varepsilon}$ is given by

$$\boldsymbol{\varepsilon}(\mathbf{x}) = \begin{cases} \boldsymbol{\varepsilon}_1(\mathbf{x}) = \nabla^{\mathrm{s}} \mathbf{u}_1(\mathbf{x}) & \text{in } \Omega_1 \\ \boldsymbol{\varepsilon}_2(\mathbf{x}) = \nabla^{\mathrm{s}} \mathbf{u}_2(\mathbf{x}) & \text{in } \Omega_2 \end{cases} \tag{3}$$

whereby the superscript s denotes the symmetric part of the differential operator. Note that the strain tensor is not defined along Γ_{I}.

3. GOVERNING EQUATIONS

We consider geometrically linear elastostatics governed by the equation of equilibrium and the boundary conditions

$$\begin{aligned} -\operatorname{div} \boldsymbol{\sigma} &= \mathbf{0} && \text{in } \Omega_1 \cup \Omega_2 \\ \mathbf{u} &= \bar{\mathbf{u}} && \text{on } \Gamma_{\mathrm{D}} \\ \boldsymbol{\sigma} \cdot \mathbf{n}_{\mathrm{e}} &= \bar{\mathbf{t}} && \text{on } \Gamma_{\mathrm{N}} \\ \boldsymbol{\sigma} \cdot \mathbf{n} &= \mathbf{t}\left([\![\mathbf{u}]\!]\right) && \text{on } \Gamma_{\mathrm{I}} \end{aligned} \tag{4}$$

To simplify matters, we assume that there are no body forces acting. $\bar{\mathbf{u}}$ is the prescribed displacement on the Dirichlet boundary and $\bar{\mathbf{t}}$ is the prescribed traction on the Neumann boundary. The Cauchy stress tensor is denoted by $\boldsymbol{\sigma}$. Cohesive tractions $\mathbf{t}$, which are calculated with a discrete constitutive law and depend on the jump in the displacement field, act along the internal boundary Γ_{I}.

Equilibrium can be expressed by means of a weak form. To this end, the equation of equilibrium (4_1) is weighted with a test function $\delta\mathbf{u}$ and after integration by parts, we obtain

$$\int_{\Omega_1\cup\Omega_2} \delta\boldsymbol{\varepsilon} : \boldsymbol{\sigma}\,\mathrm{d}V - \int_{\Gamma_{\mathrm{I}_1}} \delta\mathbf{u}_1 \cdot \boldsymbol{\sigma}_1 \cdot \mathbf{n}_1\,\mathrm{d}A - \int_{\Gamma_{\mathrm{I}_2}} \delta\mathbf{u}_2 \cdot \boldsymbol{\sigma}_2 \cdot \mathbf{n}_2\,\mathrm{d}A = \int_{\Gamma_{\mathrm{N}}} \delta\mathbf{u} \cdot \bar{\mathbf{t}}\,\mathrm{d}A \tag{5}$$

Thereby, the two sides of the discontinuity surface Γ_{I} are considered separately. We define the jump in the test function according to Equation (2) by

$$[\![\delta\mathbf{u}]\!] = \delta\mathbf{u}_1 - \delta\mathbf{u}_2 \quad \text{on } \Gamma_{\mathrm{I}} \tag{6}$$

Since equilibrium is required, $\boldsymbol{\sigma}\cdot\mathbf{n}$ has to be continuous along Γ_{I}. Taking into account the definition of the normal vector, we get $-\boldsymbol{\sigma}_1\cdot\mathbf{n}_1 = \boldsymbol{\sigma}_2\cdot\mathbf{n}_2 = \boldsymbol{\sigma}\cdot\mathbf{n} = \mathbf{t}$. Inserting this relation and relation (6) into (5), the resulting weak formulation with the additional contribution due to the tractions $\mathbf{t}$ along Γ_{I} reads

$$\int_{\Omega_1\cup\Omega_2} \delta\boldsymbol{\varepsilon} : \boldsymbol{\sigma}\,\mathrm{d}V + \int_{\Gamma_{\mathrm{I}}} [\![\delta\mathbf{u}]\!] \cdot \mathbf{t}\left([\![\mathbf{u}]\!]\right)\,\mathrm{d}A = \int_{\Gamma_{\mathrm{N}}} \delta\mathbf{u}\cdot\bar{\mathbf{t}}\,\mathrm{d}A \tag{7}$$

4. CONSTITUTIVE LAW

The material behaviour of the bulk is assumed to be linear elastic and the constitutive relation is given by

$$\boldsymbol{\sigma} = \mathbf{D} : \boldsymbol{\varepsilon} \tag{8}$$

with $\mathbf{D}$ being the fourth-order constitutive tensor. When a certain failure criterion is met, the discontinuity is introduced and the description of inelastic material behaviour is completely covered by the discrete constitutive model. This is applied at the internal boundary Γ_{I} and relates the traction vector $\mathbf{t}$ to the jump in the displacement field $[\![\mathbf{u}]\!]$.

In the following, a discrete damage-type model for quasi-brittle materials is introduced, with the tensile stress f_{t} and the fracture energy G_{f} being the main parameters; compare Reference [14]. In the direction normal to the interface, an exponential softening is assumed and, in a tangential direction, a constant shear stiffness is adopted. The traction vector $\mathbf{t}$ is determined by

$$\begin{aligned} t_n &= f_{\mathrm{t}} \exp\left(-\frac{f_{\mathrm{t}}}{G_{\mathrm{f}}}[\![u_n]\!]\right) \\ t_m &= d[\![u_m]\!] \\ \mathbf{t} &= t_n\mathbf{n} + t_m\mathbf{m} \end{aligned} \tag{9}$$

whereby d is the shear stiffness. This discrete constitutive model is chosen because of its simplicity with respect to the implementation. Due to the constant shear stiffness, the tangent stiffness matrix preserves its symmetry. Nevertheless, the introduction of a more general constitutive model is straightforward.

5. FINITE ELEMENT FORMULATION

In this section, details about the finite element discretization will be given. The weak form (7) will be solved using finite elements that allow for a discontinuity intersecting the elements following the approach suggested in References [1, 2].

5.1. Element with an internal discontinuity

To construct an element Ω^d with an internal discontinuity, we consider that Ω^d is divided by Γ_I into $\Omega_1^d := \Omega_1 \cap \Omega^d$ and $\Omega_2^d := \Omega_2 \cap \Omega^d$. The displacement field is continuous in Ω_1^d and Ω_2^d and in analogy to (1), we can describe the displacement field in the element as

$$\mathbf{u} = \begin{cases} \mathbf{u}_1 & \text{in } \Omega_1^d \\ \mathbf{u}_2 & \text{in } \Omega_2^d \end{cases} \tag{10}$$

To approximate the function $\mathbf{u}_1$ on Ω_1^d one needs the usual number of degrees of freedom, depending on the desired polynomial degree. Even though $\mathbf{u}_1$ is only defined on Ω_1^d, it can be represented by its nodal values at all nodes of the element Ω^d and the standard basis functions. The same applies for the function $\mathbf{u}_2$, which has, due to the discontinuous characteristic of $\mathbf{u}$, no relation to $\mathbf{u}_1$.

We consider, for illustration purpose, an intersected constant strain triangle, with Ω_1^d being the quadrilateral part and Ω_2^d being the triangular part. Thus, we introduce for Ω_1^d a new node j^* on the far side of Γ_I^e and for Ω_2^d, we place two new nodes, i^* and k^*, on the other side of Γ_I^e, as is pictured in Figure 2. To approximate the discontinuous displacement field $\mathbf{u}$ by means of the normal and the newly introduced global degrees of freedom, two independent copies of

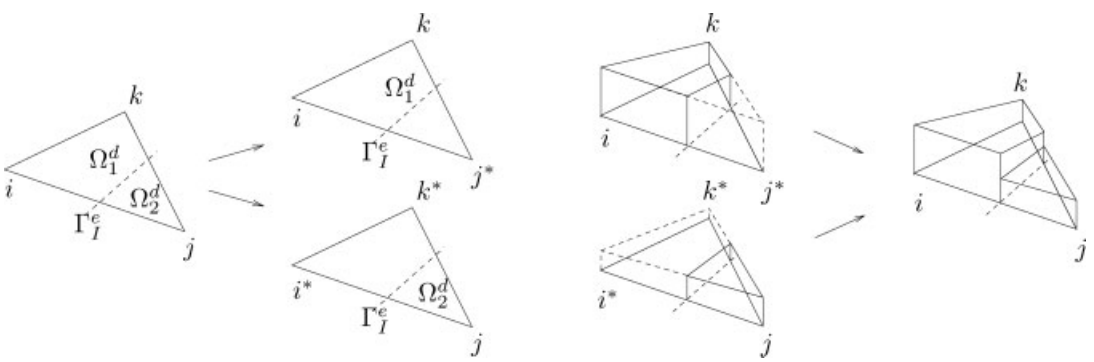

Figure 2. Split of linear triangular element and approximation of the discontinuous displacement field.

the standard basis functions are used. One set is put to zero on one side of the discontinuity, while it takes its usual values on the other side, and *vice versa*.

$$\bar{N}_1^i = \begin{cases} N^i & \text{in } \Omega_1^d \\ 0 & \text{in } \Omega_2^d, \end{cases} \quad \text{and} \quad \bar{N}_2^i = \begin{cases} 0 & \text{in } \Omega_1^d \\ N^i & \text{in } \Omega_2^d \end{cases} \tag{11}$$

Therefore, we obtain for the constant strain triangle a set of six new basis functions, three used for the approximation of $\mathbf{u}_1$ and three for $\mathbf{u}_2$. In Figure 2, the assembly of the two approximated continuous functions and the obtained discontinuous function is depicted. It is recognizable that this set of basis functions with an internal discontinuity can be easily constructed for any standard finite element in 2D or 3D. Since the additional degrees of freedom are introduced at existing nodes, the points of intersection between element edges and interface as well as the geometry of the element parts are not needed until the evaluation of the weak form.

5.2. Spatial discretization of the weak form

The elements that are not crossed by a discontinuity are usual isoparametric elements. The domain Ω is discretized into n_{el} elements. The geometry $\mathbf{x}$ is expanded elementwise by shape functions N^i in terms of the discrete nodal positions $\mathbf{x}_i$ of the $i = 1, n_{\text{en}}$ element nodes.

$$\Omega = \bigcup_e^{n_{\text{el}}} \Omega^e \quad \mathbf{x}|_{\Omega^e} = \sum_{i=1}^{n_{\text{en}}} N^i \, \mathbf{x}_i \tag{12}$$

Following the isoparametric concept, the unknown displacement field $\mathbf{u}$ is interpolated on the element level with the same shape functions in terms of the nodal displacement values $\mathbf{u}_i$. These shape functions are also applied to interpolate the test function $\delta\mathbf{u}$ in the spirit of the Bubnov–Galerkin technique

$$\mathbf{u}|_{\Omega^e} = \sum_{i=1}^{n_{\text{en}}} N^i \mathbf{u}_i \quad \delta\mathbf{u}|_{\Omega^e} = \sum_{i=1}^{n_{\text{en}}} N^i \delta\mathbf{u}_i \tag{13}$$

Based on the above discretizations the corresponding gradients $\nabla^{\text{s}}\mathbf{u}$ and $\nabla^{\text{s}}\delta\mathbf{u}$ take the format

$$\nabla^{\text{s}}\mathbf{u}|_{\Omega^e} = \sum_{i=1}^{n_{\text{en}}} \left(\mathbf{u}_i \otimes \nabla N^i\right)^s \quad \nabla^{\text{s}}\delta\mathbf{u}|_{\Omega^e} = \sum_{i=1}^{n_{\text{en}}} \left(\delta\mathbf{u}_i \otimes \nabla N^i\right)^s \tag{14}$$

The approximation of the jump in the displacement field arises automatically from the approximation of the two continuous parts of the displacement field

$$\begin{aligned} [\![\mathbf{u}]\!]|_{\Gamma_{\text{I}}^e} &= \sum_{i=1}^{n_{\text{en}^1}} N^i|_{\Gamma_{\text{I}}^e} \mathbf{u}_{1i} - \sum_{i=1}^{n_{\text{en}^2}} N^i|_{\Gamma_{\text{I}}^e} \mathbf{u}_{2i} = \sum_{p=1}^{n_{\text{en}}+n_{\text{en}}^*} M^p \mathbf{u}_p \\ [\![\delta\mathbf{u}]\!]|_{\Gamma_{\text{I}}^e} &= \sum_{i=1}^{n_{\text{en}^1}} N^i|_{\Gamma_{\text{I}}^e} \delta\mathbf{u}_{1i} - \sum_{i=1}^{n_{\text{en}^2}} N^i|_{\Gamma_{\text{I}}^e} \delta\mathbf{u}_{2i} = \sum_{p=1}^{n_{\text{en}}+n_{\text{en}}^*} M^p \delta\mathbf{u}_p \end{aligned} \tag{15}$$

Thereby, $\mathbf{u}_{1i}$ and $\mathbf{u}_{2i}$ denote the displacements at the element nodes n_{en^1} and n_{en^2}, belonging to Ω_1^d and Ω_2^d, respectively. The newly introduced term M comprises the shape functions N, evaluated on Γ_{I}^e and associated with the appropriate algebraic sign, '+' for degrees of freedom

belonging to Ω_1^d and '$-$' for those in Ω_2^d. Obviously, the jump is approximated with the same polynomial degree as the displacement field.

By means of the described discretization of the primary unknown, the weak formulation (7) is discretized and the discrete algorithmic balance of momentum follows as

$$\mathbf{R}_{\mathrm{I}}(\mathbf{u}) = \mathbf{0} \tag{16}$$

whereby the vector-valued residuum expands to the following expression

$$\begin{aligned}\mathbf{R}_{\mathrm{I}}(\mathbf{u}) = \mathop{\mathbf{A}}_{e=1}^{n_{\mathrm{el}}} \int_{\Omega^e} \nabla N^i \cdot \boldsymbol{\sigma}\, \mathrm{d}V + \int_{\Omega^d} \nabla \bar{N}_1^i \cdot \boldsymbol{\sigma}\, \mathrm{d}V + \int_{\Omega^d} \nabla \bar{N}_2^i \cdot \boldsymbol{\sigma}\, \mathrm{d}V \\ + \int_{\Gamma_{\mathrm{I}}^e} M^i \mathbf{t}\left(\llbracket \mathbf{u} \rrbracket\right)\, \mathrm{d}A - \int_{\Gamma_{\mathrm{N}}^e} N^i \bar{\mathbf{t}}\, \mathrm{d}A\end{aligned} \tag{17}$$

Herein, the operator $\mathop{\mathbf{A}}_{e=1}^{n_{\mathrm{el}}}$ denotes the assembly of all element contributions at the element nodes, including the newly introduced ones, $i = 1, n_{\mathrm{en}} + n_{\mathrm{en}}^*$ to the overall residuum at the global node points $I = 1, n_{np} + n_{np}^*$.

5.3. Linearization of the weak form

Equation (17) represents the governing discrete system of equations. Due to the applied constitutive law and the changing boundary conditions, the system of equations becomes non-linear and has to be solved iteratively. A Newton–Raphson scheme is applied and therefore a consistent linearization of the governing equations is performed

$$\mathbf{R}_{\mathrm{I}}^{k+1} = \mathbf{R}_{\mathrm{I}}^{k} + \mathrm{d}\mathbf{R}_{\mathrm{I}} = \mathbf{0} \quad \text{with } \mathrm{d}\mathbf{R}_{\mathrm{I}} = \sum_{L=1}^{n_{np}+n_{np}^*} \mathbf{K}^{\mathrm{IL}}\, \mathrm{d}\mathbf{u}_{\mathrm{L}} \tag{18}$$

whereby the iterative residuum $\mathrm{d}\mathbf{R}_{\mathrm{I}}$ is expressed in terms of the global tangent stiffness matrix $\mathbf{K}^{\mathrm{IL}}$. For the considered problem, the tangent stiffness matrix takes the format

$$\begin{aligned}\mathbf{K}^{\mathrm{IL}} = \mathop{\mathbf{A}}_{e=1}^{n_{\mathrm{el}}} \int_{\Omega^e} \nabla N^i \cdot \mathbf{D} \cdot \nabla N^l\, \mathrm{d}V + \int_{\Omega^d} \nabla \bar{N}_1^i \cdot \mathbf{D} \cdot \nabla \bar{N}_1^l\, \mathrm{d}V \\ + \int_{\Omega^d} \nabla \bar{N}_2^i \cdot \mathbf{D} \cdot \nabla \bar{N}_2^l\, \mathrm{d}V + \int_{\Gamma_{\mathrm{I}}^e} M^i \mathbf{T} M^l\, \mathrm{d}A\end{aligned} \tag{19}$$

Herein, $\mathbf{D}$ is the constitutive tensor and $\mathbf{T}$ represents the tangent stiffness of the traction separation law at the discontinuity. For the adopted constitutive relation (9), which describes exponential softening, the tangent stiffness is given by

$$\mathbf{T} = -\frac{f_{\mathrm{t}}^2}{G_{\mathrm{f}}} \exp\left(-\frac{f_{\mathrm{t}}}{G_{\mathrm{f}}} \llbracket u_n \rrbracket\right) \mathbf{n} \otimes \mathbf{n} + d\mathbf{m} \otimes \mathbf{m} \tag{20}$$

It can be easily perceived that the tangent stiffness of the traction separation law $\mathbf{T}$ retains its symmetry due to the constant shear stiffness in tangential direction.

Finally, the iterative update of the global unknown $\mathbf{u}_\mathrm{L}$

$$\mathbf{u}_\mathrm{L}^{k+1} = \mathbf{u}_\mathrm{L}^{k} + \mathrm{d}\mathbf{u}_\mathrm{L} \tag{21}$$

can be expressed in terms of the solution of the linearized equations (18).

6. IMPLEMENTATION

In this section, details about the implementation of the method are given. To describe a propagating discontinuity, we need to propose a failure criterion, a method to determine the alignment of the discontinuity and an adequate integration scheme for the intersected elements.

6.1. Propagation of the discontinuity

A discontinuity is introduced in an element when a certain failure criterion is met. During the calculation, the principle stresses in the element ahead of the tip of the discontinuity are monitored. If the stresses exceed the tensile strength f_t of the material, a discontinuity is introduced. The discontinuity is introduced as a straight line through the element and is enforced to be geometrically continuous. To determine the right direction of the extension of the discontinuity, we follow the suggestion of Wells [7]. Since the tip of the discontinuity lies on a point where the stresses are not known exactly, non-local stresses $\tilde{\boldsymbol{\sigma}}$ are calculated in view of finding the principle directions. The non-local stress tensor is computed as a weighted average of the stresses at the n_gp Gauss points within an interaction radius around the tip. A weighted Gauss function is used

$$\hat{w}(r) = \frac{1}{l\sqrt{2\pi}} \exp\left(\frac{-r^2}{[2l]^2}\right), \quad w(r) = \frac{\hat{w}(r)}{\sum_{i=1}^{n_\mathrm{gp}} \hat{w}_i A_i} \tag{22}$$

whereby r is the distance of the Gauss point to the crack tip and l determines the decline of $\hat{w}$ with respect to r. The non-local stress tensor results from the sum of the local stresses at the Gauss points i, weighted with w_i and the associated area A_i

$$\tilde{\boldsymbol{\sigma}}(\mathbf{x}) = \sum_{i=1}^{n_\mathrm{gp}} \boldsymbol{\sigma}_i w_i A_i \tag{23}$$

The discontinuity is extended in the direction perpendicular to the dominant non-local principal stress direction.

The jump in the displacement field should be continuous over the element boundaries. Therefore, the newly introduced degrees of freedom have to be global. When an additional node is introduced, it is checked, if the node has already been created by the neighbouring elements. Furthermore, the jump in the displacement field at the discontinuity tip must be equal to zero. To enforce this condition, no additional degrees of freedom are introduced at the nodes, which lie on the same element boundary as the tip of the discontinuity. In Figure 3(a), the path of the discontinuity is depicted and the additional nodes are highlighted, Figure 3(b) displays the deformation of the structure, including the additional fictitious nodes, and finally in Figure 3(c) the resulting deformation of the structure is displayed.

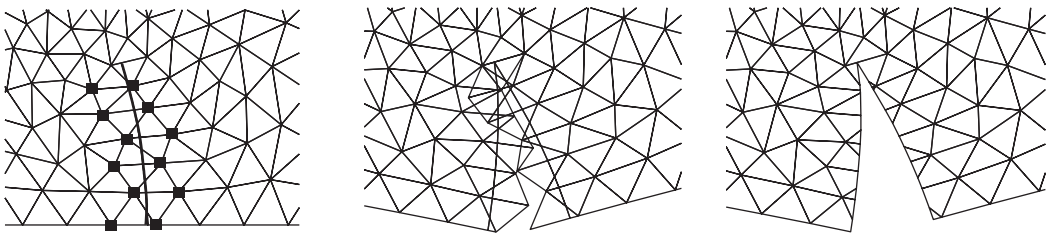

Figure 3. (a) Finite element mesh with additional nodes; (b) displacement approximation using doubled nodes; and (c) resulting discontinuous approximation.

6.2. Integration scheme

For the approximation of the displacement field of the intersected elements, the usual shape functions are used. But since the geometry of the element parts varies, the initial Gauss scheme is not valid for the intersected elements. Therefore, the quadrilateral part of the intersected element is divided into two triangles, such that three triangular subdomains are obtained. Within each triangular subdomain centroid Gaussian quadrature is applied. This approach is sufficient for constant strain triangles, for higher-order elements one needs to introduce more Gauss points for each subdomain. Additionally, two Gauss points are placed on the discontinuity surface to evaluate the terms depending on the traction forces.

7. NUMERICAL EXAMPLES

In this section, three numerical examples are presented to demonstrate the applicability of the proposed method. By means of the first example, a simple mode I failure problem, the influence of different discretizations is checked. The second example tests the method for objectivity with respect to mesh alignment and element size. Both the path of the discontinuity and the global load–displacement relation are examined for two different discretizations of a 3-point-bending beam. All examples are calculated using three-noded triangles.

7.1. Mode I failure

In the first example, purely mode I failure is considered to check the influence of different discretizations on the load–displacement relation. A square plate is loaded by a given uniform displacement at the top edge and is fixed at the bottom edge, and the geometry and the loading conditions are depicted in Figure 4. The material parameters are set to: Young's modulus $E = 100\,\mathrm{N/mm^2}$, Poisson's ratio $\nu = 0$, tensile strength $f_\mathrm{t} = 1.0\,\mathrm{N/mm^2}$ and fracture energy $G_\mathrm{f} = 0.1\,\mathrm{N/mm}$. A discontinuity is introduced at the left-hand side of the structure and is allowed to propagate through the whole specimen. Due to the bearings, which prevent a lateral movement of the structure, and due to the cohesive forces acting on the interface, the complete separation of the structure does not result in a singular tangent stiffness matrix. In Figure 6, the deformation of the plate for the three chosen discretizations with 32, 72 and 128 three-noded triangles is pictured. Since the stresses are constant, the discontinuity propagates through the whole structure, when the tensile strength is exceeded. Furthermore it propagates

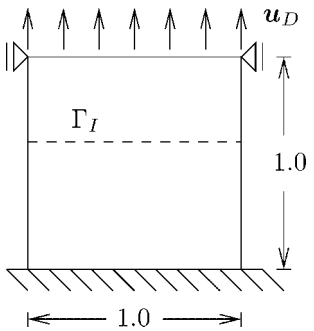

Figure 4. Geometry, loading conditions.

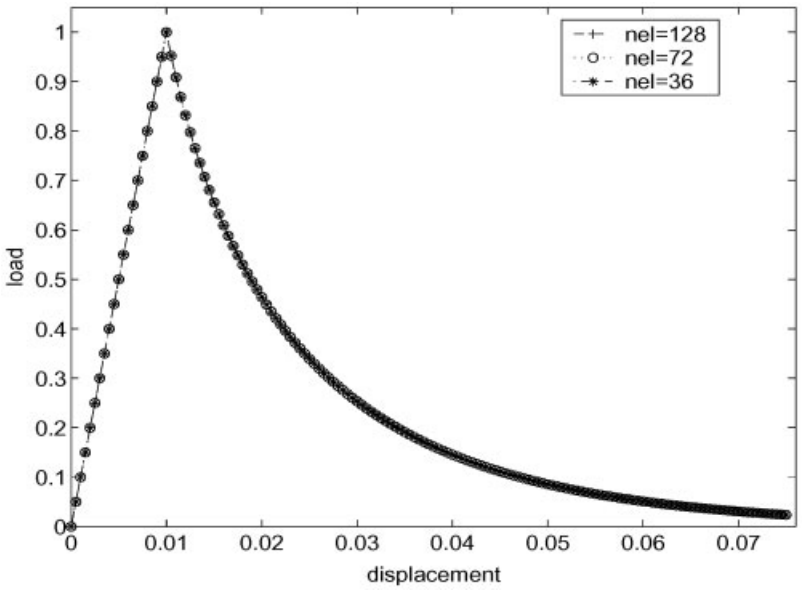

Figure 5. Load–displacement relation.

along a straight line, as expected. The load–displacement relations, which are depicted in Figure 5, confirm that the results are independent with respect to the discretization.

7.2. Three-point bending beam

We consider a three-point bending test, whereby a simply supported beam is loaded by an imposed displacement at the centre of the top edge. The following material parameters are chosen: $E = 100\,\mathrm{N/mm^2}$, $\nu = 0$, $f_\mathrm{t} = 0.5\,\mathrm{N/mm^2}$ and $G_\mathrm{f} = 0.01\,\mathrm{N/mm}$. The crack shear stiffness d is set to zero. The parameter l from Equation (22) is approximately equal to three times the average element diameter. In Figure 7, the geometry and the loading conditions are pictured. Two different unstructured meshes with 498 and 850 elements are used for the simulation.

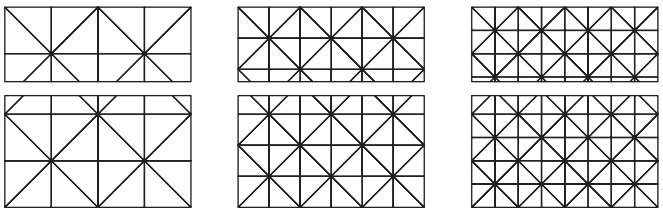

Figure 6. Deformation of the structure.

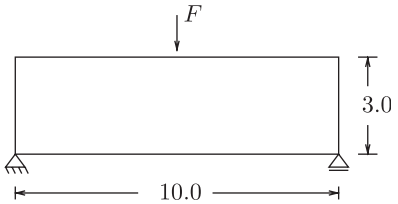

Figure 7. Geometry, loading condition.

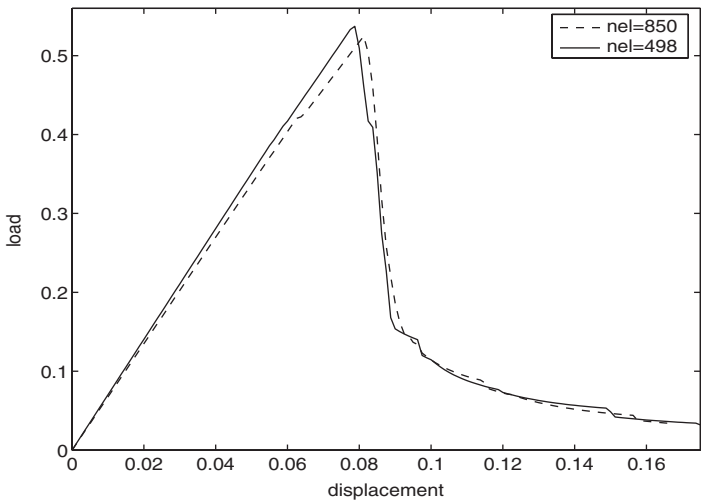

Figure 8. Load–displacement relation for centred crack.

For the first calculation, a crack is initiated at the centre of the bottom edge. As expected the crack propagates directly upwards independent of the mesh alignment. The load–displacement relations are shown in Figure 8. The peak load for the two different discretizations is slightly different. Due to the proposed failure criterion, which depends only on the maximum principal stress in the element ahead of the tip, the larger elements of the coarse mesh fail later. Therefore, the peak load is slightly overestimated for the coarse discretization. But nevertheless the good agreement of the two load–displacement curves confirms the objectivity of the method

with respect to the discretization. The path of the discontinuity is pictured in Figure 9. For both discretizations, the discontinuity describes a straight line towards the top of the beam. The path of the discontinuity is entirely independent of the mesh structure and identical for both discretizations.

In the second example, the ability of the method to model a curved crack is tested. Therefore, a concentric crack is initiated at the bottom edge of the beam (with 0.7mm offset). The crack is expected to propagate in a curved path towards the centre at the top of the beam. In Figure 11, the propagation of the crack for both discretizations is dislayed and with both discretizations the expected curved path of the crack is well described. Even the simulation with the coarse mesh gives a good approximation of the crack path, and the result cannot be distinguished from the one obtained with the fine discretization.

The load–displacement relations, pictured in Figure 10, show minor differences. The peak-load is well approximated in both cases, but the curve is quite rough for the coarse mesh. This is due to the elementwise failure. The discontinuity can only intersect the whole element at once and therefore the load–displacement relation shows small jumps. However, it is clear that for a finer discretization, these inaccuracies are smoothed out and become negligible for further mesh refinement.

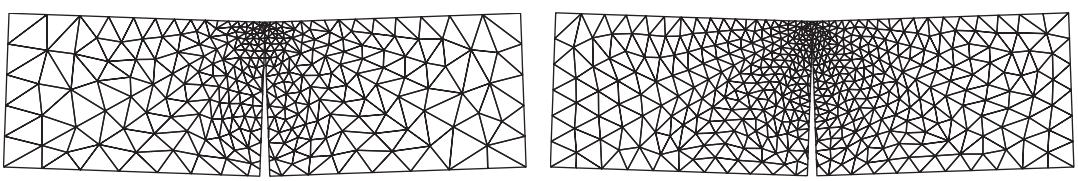

Figure 9. Propagation of the discontinuity for centred crack for both discretizations.

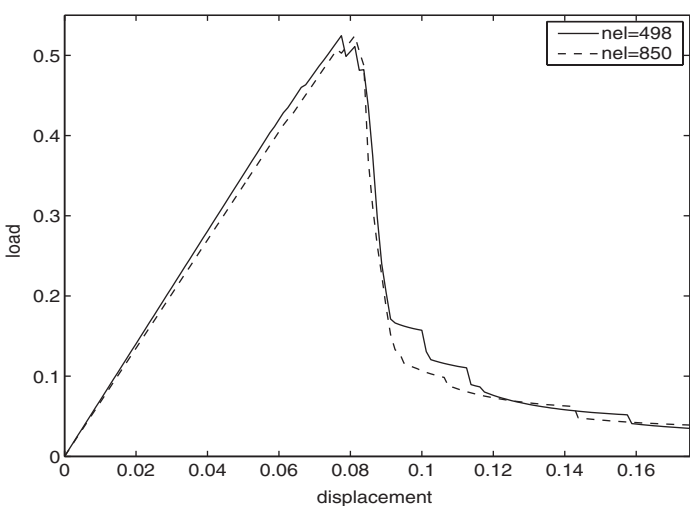

Figure 10. Load–displacement relation for excentred crack.

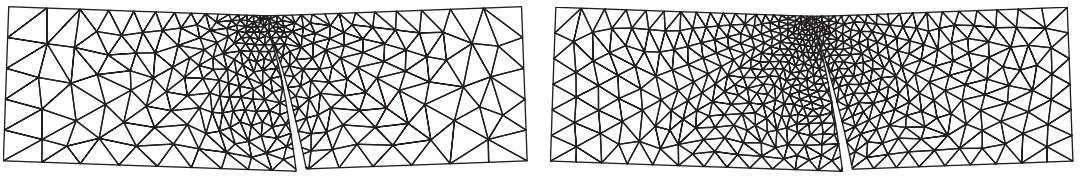

Figure 11. Propagation of the discontinuity for excentred crack for both discretizations.

8. CONCLUSION

We introduced a new finite element method for the modelling of cohesive cracks. The method allows for discontinuities propagating through the elements. The characteristic feature of the method is the construction of the elements that are intersected by the discontinuity. Additional displacement degrees of freedom are introduced at the existing nodes and only the standard basis functions are used. The manner of constructing intersected elements can be easily adapted for different elements in 2D and 3D. The method is used to model cohesive cracks. Thereby, the inelastic material behaviour is covered by a discrete constitutive law, applied at the interface. The presented numerical examples point out that the method allows for simulating propagating discontinuities, both, of straight and curved nature, independent of the mesh structure.

ACKNOWLEDGEMENTS

We gratefully acknowledge financial support by the German Science Foundation: DFG Graduiertenkolleg 814, Engineering materials on different scales: experiment, modelling and simulation.

REFERENCES

1. Hansbo A, Hansbo P. An unfitted finite element method, based on Nitsche's method, for elliptic interface problems. *Computer Methods in Applied Mechanics and Engineering* 2002; **191**:5537–5552.
2. Hansbo A, Hansbo P. A finite element method for the simulation of strong and weak discontinuities in elasticity. *Computer Methods in Applied Mechanics and Engineering*, 2004; **193**:3523–3540.
3. Babuska I, Melenk JM. The partition of unity method. *International Journal for Numerical Methods in Engineering* 1997; **40**:727–758.
4. Ortiz M, Leroy Y, Needleman A. A finite element method for localized failure analysis. *Computer Methods in Applied Mechanics and Engineering* 1987; **61**:189–214.
5. Belytschko T, Fish J, Engelmann BE. A finite element with embedded localization zones. *Computer Methods in Applied Mechanics and Engineering* 1988; **70**:59–89.
6. Jirásek M, Zimmermann T. Embedded crack model. Part I: basic formulation. *International Journal for Numerical Methods in Engineering* 2001; **50**:1269–1290.
7. Wells GN. Discontinuous modelling of strain localisation and failure. *Ph.D. Thesis*, Technische Universiteit Delft, Delft, The Netherlands, 2001.
8. Armero F, Garikipati K. An analysis of strong discontinuities in multiplicative finite strain plasticity and their relation with the numerical simulation of strain localization in solids. *International Journal of Solids and Structures* 1996; **33**:2863–2885.
9. Oliver J, Huespe AE, Pulido MDG, Samaniego E. On the strong discontinuity approach in finite deformation setting. *International Journal for Numerical Methods in Engineering* 2003; **56**:1051–1082.
10. Belytschko T, Black T. Elastic crack growth in finite elements with minimal remeshing. *International Journal for Numerical Methods in Engineering* 1999; **45**:601–620.

11. Moës N, Dolbow J, Belytschko T. A finite element method for crack growth without remeshing. *International Journal for Numerical Methods in Engineering* 1999; **46**:131–150.
12. Sukumar N, Möes N, Moran B, Belytschko T. Extended finite element method for three-dimensional crack modeling. *International Journal for Numerical Methods in Engineering* 2000; **48**:1549–1570.
13. Daux C, Moës N, Dolbow J, Sukumar N, Belytschko T. Arbitrary branched and intersecting cracks with the extended finite element method. *International Journal for Numerical Methods in Engineering* 2000; **48**:1741–1760.
14. Wells GN, Sluys LJ. A new method for modelling cohesive cracks using finite elements. *International Journal for Numerical Methods in Engineering* 2001; **50**:2667–2682.
15. Zi G, Belytschko T. New crack-tip elements for XFEM and applications to cohesive cracks. *International Journal for Numerical Methods in Engineering* 2003; **57**:2221–2240.
16. Nitsche J. Über ein Variationsprinzip zur Lösung von Dirichlet-Problemen bei Verwendung von Teilräumen, die keinen Randbedingungen unterworfen sind. *Abhandlungen aus dem Mathematischen Seminar der Universität Hamburg* 1970; **36**:9–15.

